Z. Physik 264, 427—444 (1973)

Precision Neutron Total Cross Section Measurements on Gold and Cobalt in the 40 μeV–5 meV Range

W. Dilg, W. Mannhart, E. Steichele and P. Arnold

Physik-Department der Technischen Universität München, Garching

Received July 18, 1973

The slow neutron absorption cross sections of gold and cobalt have been accurately redetermined by transmission measurements in the neutron wavelength range 4 to 47 Å. For the range 4 to 7.6 Å a new time-of-flight spectrometer at the FRM reactor was used which involves a system of three synchronized choppers and a 150 m long guide tube as flight path. Utilizing the high wavelength resolution of the spectrometer, the time-of-flight wavelength scale could be accurately calibrated ($\pm 2 \cdot 10^{-3}$ Å) by means of various Bragg cutoff breaks observed in transmission on polycrystalline samples. Supplementary transmission measurements on gold and cobalt were performed in the range 11–47 Å using the time-of-flight spectrometer for ultracold neutrons at the FRM reactor.

The absorption cross sections were evaluated considering corrections for incoherent and inelastic scattering and for the slight deviation from $1/v$ of the absorption of gold due to the 4.9 eV resonance level. For the absorption at subthermal energies we obtain $\sigma_a/\lambda = (54.35 \pm 0.06)$ b/Å for Au, (20.66 ± 0.04) b/Å for Co. Evaluation of the absorption cross sections at 2200 m/s neutron velocity gives (98.68 ± 0.12) b for Au, (37.15 ± 0.08) b for Co.

I. Introduction

The use of standard cross sections is necessary in many experiments with slow neutrons such as measurements of neutron flux and absorption cross sections, activation analysis etc. The most frequently used thermal neutron *activation* standards are the capture cross sections of gold and cobalt, which activate with convenient half lives and have well-known decay schemes.

The best known thermal absorption cross sections are presently those of gold and ^{10}B determined absolutely by transmission measurements at long wavelengths where scattering contributions to the total cross sections become small. Recommended values, [1–3], as well as the most precise single measurements, [4–7] are accurate to about 0.3%. In future applications, however, even more precise values of these standards might be of interest; for example, in a request (WRENDA 73 [8]) from JNDC the thermal capture cross section of gold is desired with an accuracy of 0.1% for standardization of thermal neutron flux density measurements.

In the previous experiments on gold, which were performed with crystal spectrometers [4, 6] and the time-of-flight method [5, 9], the principal sources of error were the wavelength measurement and statistics. The wavelength calibration was mostly done with Bragg cutoffs observed on polycrystalline samples in transmission. As discussed by Gould *et al.* [4] and Carter *et al.* [9], the accuracy of this calibration procedure is practically limited by the wavelength resolution of the spectrometer. Resolutions $\Delta\lambda/\lambda$ of 2–4% were used in [4, 9] and the systematic uncertainty of the wavelength scale was estimated to be 0.2–0.3%. No details about resolution were given by Als-Nielsen and Dietrich [6], but a 0.2% overall accuracy and a 0.06% wavelength uncertainty were claimed. Actually, however, their (σ_a/λ) data show a marked wavelength trend of about 1% from 5 to 8 Å.

Previous measurements of the cobalt absorption cross section have been recently reviewed by Silk and Wade [10]. Most of the data are related to gold or boron using activation and pile oscillator methods. There is only one precise absolute determination [10] using the pulsed neutron technique. Available data based on transmission measurements [11, 12] are rather old and contradictory. Besides that, these experiments covered only the neutron energy range above 30 meV where, in ferromagnets as in cobalt, one has elastic magnetic scattering in addition to the usual coherent elastic scattering.

In this paper we report transmission measurements in the meV energy region using a new thermal neutron time-of-flight (TOF) spectrometer at the FRM reactor in Garching. This facility, which is primarily designed for high resolution neutron diffraction work [13], uses as flight-path a 150 m long totally reflecting curved neutron guide tube. Thus, one obtains low background in an experimental area far from the reactor and above all such a high wavelength resolution that the contribution of the wavelength error to the total error becomes negligible compared to other uncertainties. In spite of its length, the guide tube provides sufficient intensity in the range $\lambda = 4$–8 Å, which is desirable for transmission measurements on solid samples to avoid corrections for Bragg scattering.

II. Total Cross Sections for Wavelengths 4–7.6 Å

II.1. TOF Spectrometer

The spectrometer consists of the above-mentioned neutron guide tube [14], and a system of three synchronized choppers near the reactor. The design considerations of the instrument, which were given by the normal application to neutron diffraction work, will be described else-

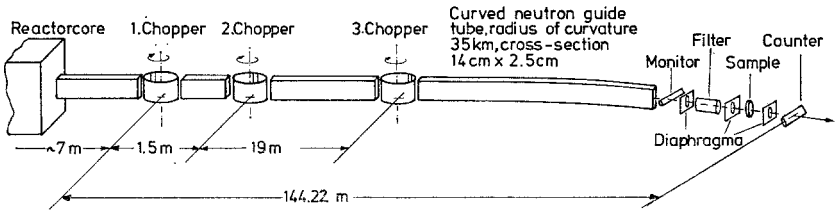

Fig. 1. Schematic diagram of the TOF spectrometer: three-chopper system, curved neutron guide tube as flight path, arrangement of the transmission experiment

where [13]. In the present context we will outline only the main characteristics. The principal set-up is shown in Fig. 1.

The guide tube begins at about 1 m from the reactor surface and has a cross-section of 14 cm × 2.5 cm. Being designed for transmission of neutrons with a wavelength of about 1 Å, the first part with a length of 100 m is curved in the horizontal plane with a radius of 35000 m. Due to the curvature, beyond this distance of 100 m from the reactor, there is no direct path from any point of the beam cross-section to the reactor core. Therefore, the thermal beam, which *follows* the guide tube, is contaminated only by background radiation (fast neutrons, γ-rays) which has been *scattered* in the walls of the tube. The distance from the detector at the end of the guide tube to any possible source of background radiation is therefore at least 50 m and for this reason the background is very low.

The guide tube is constructed from rectangular tubes 1 m in length, made of nickel-coated glass plates and adjusted in evacuated steel tubes with an accuracy of $\sim 1 \times 10^{-4}$ rad ($\sim 20''$).

The collimation of the beam in horizontal and vertical directions is determined by the critical angle for total reflection, which is wavelength dependent and is related to the coherent scattering length a_{coh} of the mirror and the number N of scattering atoms per unit volume by:

$$\gamma_c = \sqrt{\frac{N \cdot a_{\mathrm{coh}}}{\pi}} \cdot \lambda.$$

With nickel as a mirror one gets $\gamma_c = 6'$ for neutrons with 1 Å. Thus, the collimation of the primary beam is 1.4×10^{-2} rad for 4Å and 2.8×10^{-2} rad for 8 Å, respectively.

The total flux (without choppers) at the end of the guide tubes is $\sim 2.5 \times 10^6$ n/cm^2 sec. In Fig. 2 we show the spectral distribution and (cross-hatched) the region of the spectrum we used for the measurements.

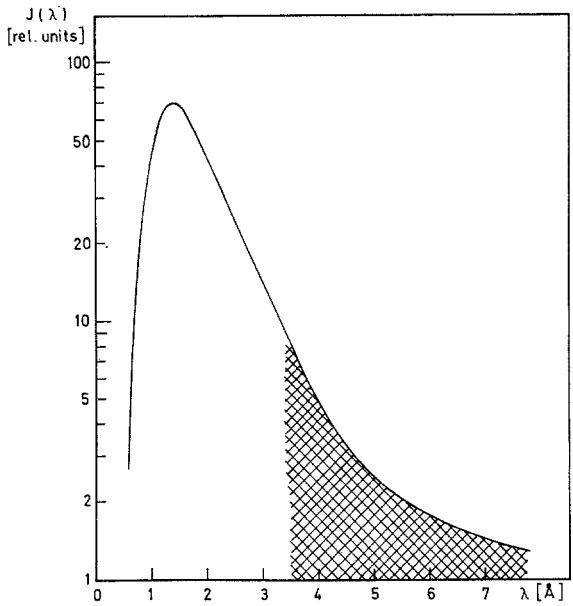

Fig. 2. Primary spectrum (without choppers) at the end of the neutron guide tube. The integral flux (without choppers) is about $2.5 \cdot 10^6$ n/sec · cm^2. The cross-hatched part indicates the spectral region used in the present measurements

The selection of appropriate wavelength regions is done with the three-rotor chopper system, the principal function of which is the following: The first chopper forms a white pulse and its time-width defines the TOF resolution. The second and third choppers act as "tail cutters" and define the width and the center of the wavelength distribution transmitted by the system. The center of this spectrum can be shifted by changing the relative phases between the choppers and the width can be changed by changing the velocity ratios. The positions of the choppers (see Fig. 1) are chosen in a way that there is no frame overlap between two successive pulses for any frequency ratio and phase. The rotors of the choppers consist of aluminum cylinders (350 mm diameter, 160 mm high) with vertical axes, the inner walls ($\sim$2 mm thick) of which are coated with a 0.5 mm layer of Cd. Two vertical slits 30 mm in width in this Cd layer act as chopper slits. If the chopper is closed, the transmission of one rotor for neutrons with wavelengths longer than 0.6 Å is $\sim 10^{-5}$. The rotors are driven by synchronous motors with velocities between 200 and 8500 rpm. The phase jitters of the running choppers relative to the synchronized input signals are less than 1°.

II.2. Transmission Geometry

The experimental set up at the end of the guide tube is illustrated in detail in Fig. 3. A $B^{10}F_3$ counter (1″ ∅) mounted at the upper edge of the guide tube exit was used as an integral flux monitor. Before passing the sample, the beam was filtered through a 90 mm long beryllium polycrystal (at room temperature) in order to reduce any background of neutrons with wavelengths shorter than 0.6 Å, for which the choppers are not completely "black". The transmission of the filter for those wavelengths is estimated to be 0.3%. Together with the partial absorption in the choppers and the low intensity in the incoming beam, the remaining background of these short wavelength neutrons was negligible. The transmission of the filter for long wavelength neutrons was 70% for 4 Å and 55% for 7.6 Å, respectively. While the divergence of the incoming beam is determined by the guide tube, four Cd-diaphragms define the diameter of the beam and avoid the effect of in-scattering of neutrons into the detector.

With a geometrical divergence of 1.6° from the sample to the exit diaphragm, this solid angle is of the order of 5×10^{-4}. The alignment of the different parts was done with a laser beam. The sample-holder axis had a maximum deviation of 0.5° from the main beam axis. Thus the error in sample thickness due to oblique transmission is also negligible. Transmitted neutrons were detected in a $B^{10}F_3$ counter (2″ ∅, 20 cm active length, measured dead-time 3.1 μsec), the axis of which was set perpendicular to the beam axis. The error in the length of the flight-path due to finite detector thickness is negligible. The detector counts were stored in different subgroups of a 4096 channel analyzer operating in the multiscaling mode.

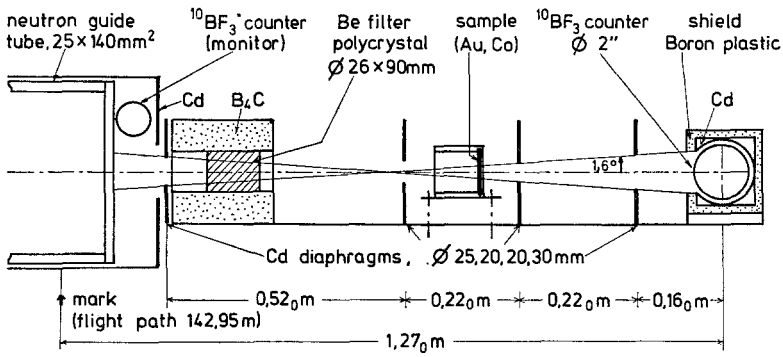

Fig. 3. Schematic drawing of the arrangement for the transmission measurements

II.3. Samples

Two samples of gold* (purity 99.999%), 0.88 and 1.00 mm thick, and one sample of cobalt** (15 ppm metallic impurity), 1.02 mm thick were used. The samples were machined to discs with diameters of about 28 mm. From the weights and the diameters we obtained the mean values of grams per cm^2 for each sample with an error less than 0.02%. Additional direct measurements of the thickness at many points on the sample area using a micrometer showed, that the quadratic effect of sample thickness fluctuations [15, 4] was negligible. However, a systematic variation of a few microns from the center to the periphery was found for the cobalt sample and one of the gold samples. This was corrected for in calculating the grams per cm^2 and atoms per barn for the central area of 20 mm $\varnothing$ of the samples, which was effectively used in the transmission measurement. With estimated errors from this correction the resulting n (atoms/barn) were $(5.1271 \pm 0.0025) \cdot 10^{-3}$ and $(5.8505 \pm 0.0012) \cdot 10^{-3}$ for gold and $(9.164 \pm 0.005) \cdot 10^{-3}$ for cobalt.

II.4. Measurements

The measurements were performed in one run of about 8 hours for cobalt and in two runs of each about 100 hours for gold during different reactor periods. The experimental conditions were practically the same. The total wavelength range from 3.4 to 7.6 Å was scanned in two and three steps, respectively, to get about the same statistical error for wavelengths regions of different primary intensity. The different combinations of chopper velocities and some experimental characteristics are shown in Table 1.

For each spectral range the channel-to-wavelength calibration had to be established. This was done by means of various Bragg cutoff breaks observed in transmission on Pb, Si, Be, Fe and Mg; the corresponding cutoff wavelengths (Table 1) were calculated from the well-known lattice constants [16]. The raw data of some typical calibration measurements are shown in Fig. 4a–d. Part a) shows the primary spectrum between 3.4 and 6.1 Å. The break is due to some aluminum windows in the spectrometer. Parts b) and c) show the spectrum transmitted through iron and lead powder samples; part d) shows the beryllium-filtered beam. Expanded plots of the transmission as a function of wavelength near the Bragg cutoff are shown in Fig. 5. From the rise of the cutoff which results from the convolution of the actual more step-like transmission with the instrumental resolution one gets the upper limit of the resolution.

---

* From Degussa, Hanau, Fed. Rep. of Germany.
** From Johnson and Matthey, Great Britain.

Table 1

	Chopper frequencies rpm	TOF-unit	Wavelength resolution *FW*	Wavelength range Å	Aprox. total intensity		Wavelength calibration
					beam cts/min	background cts/min	
1st run	$f_1=1923.0$	1024 channels	0.012 Å	(I) 3.4–6.1	9000	1.4	Be (100), Fe (110), Mg (011), Pb (111), (200)
	$f_2=f_1/2$	100 μsec/channel	(~450 μsec)				
	$f_3=f_1/10$	~0.0027 Å/chan.		(II) 4.7–7.4	4800	1.7	Pb (111), Si (111)
2d run	$f_1=3125.0$	256 channels	0.008 Å	(III) 4.8–6.1	5700	2.9	Pb (200), (111)
	$f_2=f_1/3$	200 μsec/channel	(~300 μsec)	(IV) 5.3–6.6	3800	3.5	Pb (111), Si (111)
	$f_3=f_1/6$	~0.0055 Å/chan.		(V) 6.3–7.6	2000	3.3	

The wavelengths of the different Bragg cutoffs used for the calibration are:

Be (100): 3.960_6 Å; Fe (110): 4.053_8 Å; Mg (011): 4.904_5 Å; Pb (200): 4950_5 Å; Pb (111): 5.716_2 Å; Si (111): 6.270_8 Å.

The total length of the flight path was $L_0=144.98$ m for the first run and $L_0=144.22$ m for the second run.

The width, indicated in Fig. 5 is in good agreement with the resolution expected from the instrumental parameters.

The positions of the Bragg cutoffs were determined as the channel numbers of the half-value transmission $(T_< + T_>)/2$ with estimated errors of 0.3 channels $\cong 1 \cdot 10^{-3}$ Å. Thus we got six calibration points which we found to be consistent within 2×10^{-3} Å with the TOF calibration using the data for the length of the flight path, the channel time and the delay time of the TOF unit. The stability of the TOF calibration was proved by numerous short measurements, of about one hour, with the proper powder samples. Thus we estimate an overall accuracy in our wavelength calibration of $\pm 2 \times 10^{-3}$ Å giving a relative error of 0.03% for $\lambda \sim 6$ Å.

In the measurements on gold and cobalt, sample-in and sample-out spectra were recorded in periods of 15 min and added in different subgroups of the multichannel analyzer. Data collected during 4 hours were evaluated separately. Monitor counts for the corresponding periods

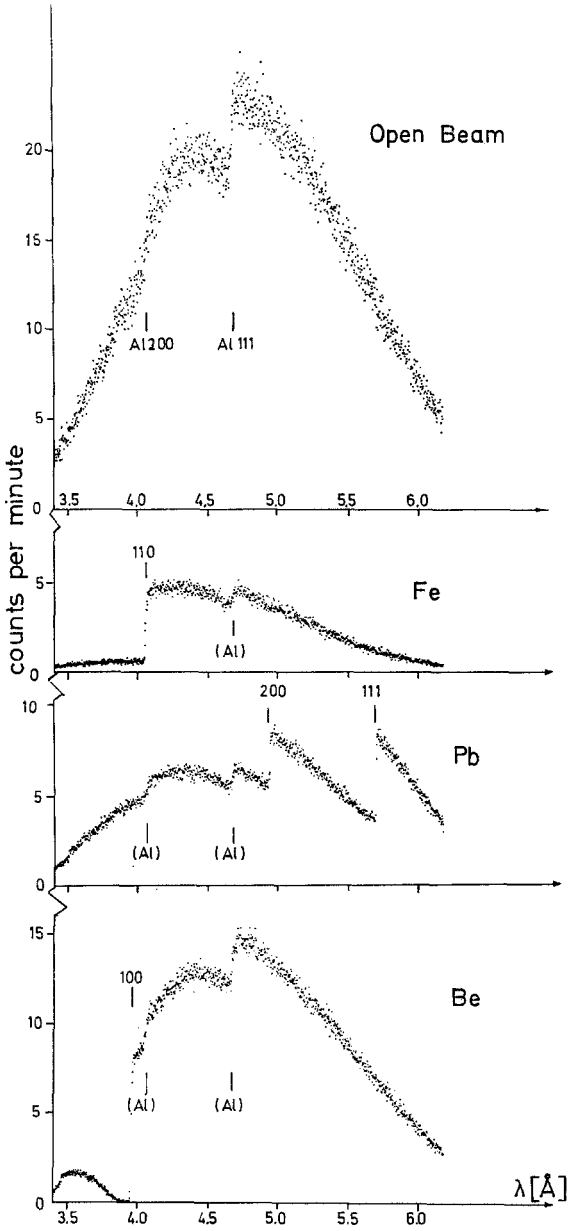

Fig. 4. Wavelength calibration of the TOF scale by means of Bragg cutoff breaks. The plotted data were obtained with spectrum I, 1st run (see Table 1); open beam: 30 min; Fe: 90 min; Pb and Be: 120 min. The structure in the open beam spectrum is due to some aluminum windows in the spectrometer

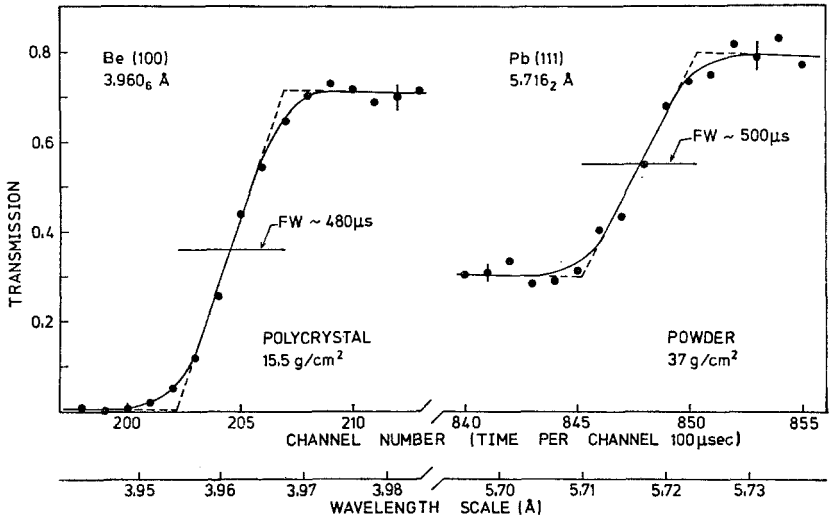

Fig. 5. Expanded plot of the transmission near the Be (100) and the Pb (111) cutoffs showing the experimental resolution

were added and used to correct for flux variations. These corrections were typically 0.5 to 1%.

II.5. Data Analysis and Results

The TOF spectra were analyzed by means of a computer code to evaluate for each channel: (1) the wavelength; (2) the total cross section with standard error; (3) the cross section normalized to the wavelength and reduced by corrections (see below) for incoherent scattering, inelastic scattering and (for gold) the non-λ proportional absorption at the corresponding wavelength, i.e., $(\sigma_{\text{tot}}-\sigma_{\text{inc}}-\sigma_{\text{ie}}-\sigma_{\text{non-}\lambda})/\lambda$. The latter values were then averaged over a range of ~0.1 Å. Including all measurements this first data reduction yielded about 400 such means for gold and 24 values for cobalt, with typical standard errors of 0.5–1.0%.

II.5.1. Gold, 4–7.6 Å

In the evaluation of the absorption only data for wavelengths above the (111) Bragg cutoff at 4.71 Å were considered. The cross sections observed at shorter wavelengths include contributions from Bragg scattering which depend critically on details of the structure of the particular sample such as grain size and orientation. The rise of the coherent contribution, for gold of the order 2.5% near the cutoff, was

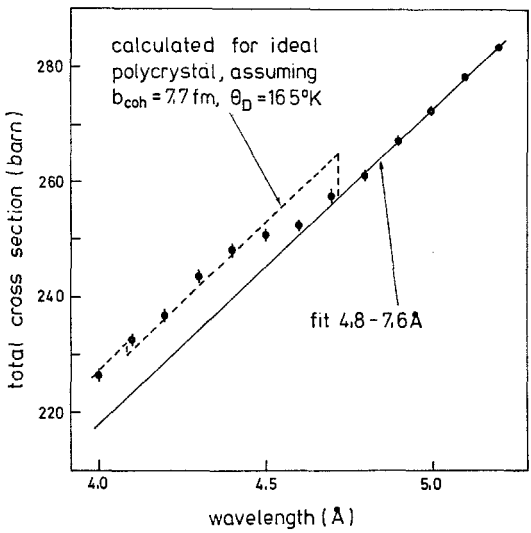

Fig. 6. Observed total cross-sections of (cast) gold near the 4.71 Å cutoff. The full line represents the fit to the long wavelength data. The dashed line is calculated by adding the contribution of Bragg scattering as obtained from the standard formula (Weiss [18]) for *ideal* polycrystals (grain size $\lesssim 10^{-4}$ cm, random orientation). With the cast samples used in the present experiment the cutoff did not appear as a sharp break; somewhat below 4.71 Å, however, the observed effect is of the expected magnitude

clearly seen in the present measurement (Fig. 6) but did not appear as a sharp break. For cast material this smearing out is well known [17, 18] as the combined effect of extinction and non-random grain orientations.

At wavelengths above the cutoff, the total cross sections are given by

$$\sigma_{tot} = \sigma_a + \sigma_{inc} + \sigma_{ie}, \tag{1}$$

where the remaining contributions of spin incoherent elastic and thermal inelastic scattering are each of the order 0.1%. For the incoherent cross section the value $\sigma_{inc} = (0.50 \pm 0.26)$b was reported by Brockhouse [19]. The inelastic cross section varies as λ at subthermal energies and can be estimated theoretically in the incoherent approximation for the Debye model [20, 21, 4] as $\sigma_{ie} \simeq 0.030 \cdot \lambda \cdot \text{barn} \cdot \text{Å}^{-1}$. The estimation should be correct within $\pm 30\%$ [21]. – The major absorption terms is expected to be strictly proportional to λ at long wavelengths, however, at meV energies the 4.906 eV resonance level introduces a small non-λ variation in the cross section. Its magnitude [4] $1.70 \cdot \lambda^{-1} \cdot \text{barn} \cdot \text{Å}$ ($\pm 4\%$), is readily calculated with the resonance parameters of Wood *et al.* [22] as

Table 2. Results. Numbers in brackets give the estimated wavelength error and the standard errors of σ_{tot} and $(\sigma_a/\lambda)_0$, respectively

λ (Å)	E (meV)	Gold		Cobalt	
		σ_{tot} (b)	(σ_a/λ) (b/Å)	σ_{tot} (b)	σ_a/λ (b/Å)
		Wavelength range 4.7–7.6 Å			
4.800 (2)	3.550	261.2 (9)	54.21 (19)		
4.900 (2)	3.407	267.3 (6)	54.35 (13)		
5.000 (2)	3.272	272.6 (5)	54.32 (10)		
5.100 (2)	3.145	278.4 (4)	54.40 (8)		
5.200 (2)	3.025	283.5 (4)	54.33 (8)		
5.350 (2)	2.858	291.7 (4)	54.34 (7)		
5.600 (2)	2.608	304.9 (3)	54.28 (5)	120.7 (6)	20.51 (13)
6.000 (2)	2.272	326.5 (4)	54.26 (7)	129.5 (5)	20.60 (8)
6.500 (2)	1.936	355.1 (6)	54.49 (9)	141.4 (7)	20.84 (11)
7.000 (2)	1.669	382.7 (7)	54.54 (10)	151.3 (7)	20.76 (10)
7.500 (2)	1.454	408.5 (12)	54.34 (16)	160.8 (12)	20.65 (16)
		Wavelength range 11–47 Å			
13.15 (4)	0.473	716.7 (33)	54.43 (25)	280.4 (20)	20.86 (15)
16.69 (4)	0.294	907.8 (41)	54.33 (25)	352.5 (18)	20.75 (11)
20.24 (4)	0.200	1104.4 (50)	54.51 (25)	423.7 (20)	20.62 (10)
23.79 (5)	0.1445	1299.4 (57)	54.57 (24)	496.5 (21)	20.60 (9)
27.35 (5)	0.1094	1486.7 (66)	54.31 (24)	571.4 (28)	20.65 (10)
30.92 (5)	0.0856	1699.2 (77)	54.91 (25)	647.0 (31)	20.71 (10)
34.49 (5)	0.0688	1890.6 (93)	54.77 (27)	713.3 (38)	20.48 (11)
38.08 (5)	0.0564	2077 (11)	54.50 (29)	788.2 (50)	20.51 (13)
41.67 (6)	0.0471	2246 (13)	53.86 (32)	864.9 (58)	20.58 (14)
45.28 (6)	0.0399	2460 (19)	54.29 (36)	945.6 (77)	20.72 (17)

the first correction term obtained by expanding the single level Breit-Wigner formula at zero energy.

To obtain the long wavelength limit of the absorption $(\sigma_a/\lambda)_0$ we analyzed our data using the following three procedures:

a) Adopting the corrections as given above, $(\sigma_a/\lambda)_0$ was determined as the weighted mean of the 383 values σ_{corr}/λ^i. The overall average with standard error was (54.344 ± 0.024)b/Å. A χ^2 test gave $\chi^2 = 388$, probability 41%. The combined additional error due to the corrections is about 0.05 b/Å.

To check the sample thickness determination the weighted means were also evaluated separately for the two samples. The results, 54.33(4) and 54.36(4), agreed well within the standard errors. Thus we summarized the data of both samples over different wavelength ranges of 0.1 to 0.5 Å width to check them for a possible wavelength trend. These means are given in Table 2 and plotted in Fig. 7. The plot also shows previous

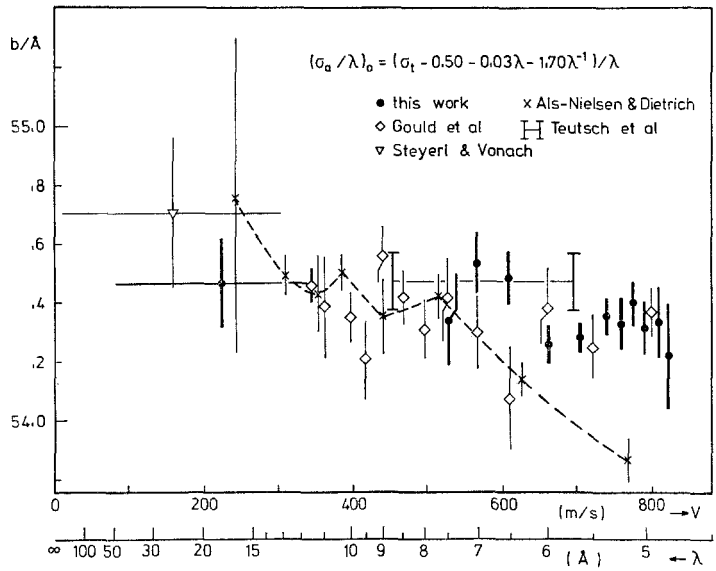

Fig. 7. Absorption of gold, normalized per Angstrom. The plot shows the means over the different wavelengths intervals within the range 4.7–7.6 Å (Table 2), as well as the mean of the data in the range 11–47 Å. Previous results are also given for comparison. Data of Als-Nielsen and Dietrich [6] are connected by the dashed line showing the strong trend at the shorter wavelengths

results which had been corrected in the same way. Our results agree well with those of Gould *et al.* [4], Teutsch *et al.* [5] and those of Als-Nielsen and Dietrich [6] above 7 Å. However, our data do not support the marked trend seen by the latter authors at the shorter wavelengths. This systematic deviation from $1/v$, eight times the quoted standard errors, is probably due to errors of the wavelength measurements*.

b) A least square fit $a+b\cdot\lambda$ to the total cross sections was performed with the result listed in Table 3. Because of the relatively small wavelength range covered by our measurement, both the slope and the intercept at $\lambda=0$ are rather inaccurate and do not provide a significant interpretation with respect to absorption and incoherence. Corresponding fits by Gould *et al.* [4] and Teutsch *et al.* [5] have led to similar conclusions, and their final estimates were therefore based on evaluation (a).

c) The main uncertainty in procedure a) is due to the experimental value of the incoherence; thus a consistency check with the long wavelength data was desirable. For that purpose, we performed another

* The He^3 cross section data of Als-Nielsen and Dietrich [6] show the same trend to low values at 6.35 and 5.17 Å.

Table 3. Comparison with previous results for gold. Standard errors are given in columns 3–5; errors of $\sigma_a(2200)$ include also systematic experimental uncertainties and errors of the scattering corrections

	λ range (Å)	Evaluation			σ_a (2200 m/s) (barn)
		(a) $(\sigma_a/\lambda)_0$	(b) fit σ_t	(c) fit $\sigma_t - 1.7 \cdot \lambda^{-1}$	
Carter *et al.* [9]	5 — 9	54.40 (25)			98.7 (6)
Gould *et al.* [4]	5 — 11.5	54.40 (3)	$-0.46\,(67)+$ $+54.56\,(9)\cdot\lambda$		98.8 (3)
Teutsch *et al.* [5]	5.7— 8.8	54.47 (10)	$+3.6+54.06\cdot\lambda$		98.9 (3)
Als-Nielsen and Dietrich [6]	5 — 16	54.32 (8)			98.6 (2)
Steyerl and Vonach [28]	15 —500				99.3 (5)
This work	4.7— 7.6	54.344 (24)	$-0.84\,(1.32)+$ $+54.66\,(24)\cdot\lambda$	$+0.43\,(26)+$ $+54.387\,(52)\cdot\lambda$	98.68 (12)
	11 — 47	54.46 (9)		↓ slope-σ_{ie}: 54.357 (52)	

weighted least squares fit $a'+b'\cdot\lambda$ to the 383 cross sections corrected only for the non-λ absorption term, $\sigma_{tot}-1.70\cdot\lambda^{-1}$; in this fit we included also the experimental incoherence (0.50 ± 0.26) b as an additional input value at $\lambda=0$. The result given in Table 3 shows that the inclusion of this point considerably improves the accuracy of both a' and b'. The χ^2 of the fit was nearly the same as that obtained with evaluation (a); the fitted a' is only slightly less than the experimental σ_{inc} and consistent within error. Subtracting the inelastic contribution from the slope b' gives $(\sigma_a/\lambda)_0=(54.357\pm0.052)$ b/Å. The error obtained in this way includes both statistics and the uncertainty of the incoherence. Additional errors due to the inelastic scattering and Breit-Wigner correction are relatively small (0.03%) as are the principal experimental uncertainties of sample thickness (0.04%) and wavelength measurement (0.03%).

Thus our final estimate for gold is

$$(\sigma_a/\lambda)_0=(54.35\pm0.06)\ \text{b/Å}$$

based on the evaluations a) and c) the results of which are in close agreement.

II.5.2. Cobalt, 5.4–7.6 Å

The cobalt cross sections are given in Table 2 averaged over the same wavelength ranges as the gold data. The absorption was assumed to be strictly proportional to λ and was evaluated again on the basis of Eq. (1).

Elastic magnetic scattering is not present above the cutoff in ferromagnets like cobalt; the cross section for inelastic magnetic scattering was estimated theoretically [21] as <0.1 b ($T=300$ °K; $E\sim$meV). The estimate for thermal inelatic scattering gives $\sigma_{ie}\simeq 0.034\cdot\lambda\cdot\text{barn}\cdot\text{Å}^{-1}$ ($\pm 30\%$). Thus the main correction, about 4%, is for spin-incoherent scattering.

For cobalt σ_{inc} can be determined as

$$\sigma_{inc}=((A+1)/A)^2\cdot\sigma_s-\sigma_{coh},$$

since the (bound) coherent cross section $\sigma_{coh}=(0.79\pm 0.06)$ b [23, 24] is sufficiently small and well known. However, published data of the (free) scattering cross section σ_s, (6.7 ± 0.3) b [11] and (5.0 ± 0.5) b [12], are contradictory. To remove that uncertainty we measured additionally the total cross section of cobalt at 1.25 eV neutron energy. We used an experimental set up at the FRM reactor developed for accurate transmission measurements by means of rhodium resonance detectors [25, 26]. The result was $\sigma_{tot}(1.25\text{ eV})=(10.7\pm 0.2)$ b. Correcting for the absorption at 1.25 eV, we find $\sigma_s=6.3$ b, and $\sigma_{inc}=(5.7\pm 0.3)$ b.

The further evaluation of the absorption was done using the procedures a) and c) as described for gold. The two results of σ_a/λ were in close agreement, the mean being

$$\sigma_a/\lambda=(20.67_5\pm 0.06)\text{ b/Å}.$$

The error includes statistics ($\sim 0.22\%$) and the principal systematic uncertainty ($\sim 0.2\%$) due to the correction for incoherent scattering.

III. Total Cross Sections for Wavelengths 11–47 Å

Additional measurements were performed using the time-of-flight spectrometer for ultracold neutrons (Steyerl [27]) at the FRM reactor. This facility covers the neutron velocity range from 5 to 350 m/s, the maximum intensity being available near 140 m/s, i.e. 28 Å. At these wavelengths incoherent scattering is further reduced compared with capture and the error for the absorption due to the corresponding corrections becomes negligible.

A previous measurement on gold using that spectrometer (Steyerl and Vonach [28]) gave $\sigma_a(10\text{ m/s})=(21\,650\pm 100)$ b, i.e. $\sigma_a/\lambda=(54.72\pm 0.25)$ b/Å, the given uncertainty being three times the standard error. Thus the deviation from our results presented in Section II cannot be considered as merely statistical. A very probable source of systematic error could be the mass thickness of the thin foils used as samples (thickness variations $\pm 5\%$ as stated in [28]).

The present measurement was restricted to the velocity range ~ 80 to 350 m/s providing the best intensity conditions and allowing the use of thicker samples. Since the details of the spectrometer have been described previously [27] we summarize here only the main data concerning our experiment. A duty cycle period of 1.16 sec was used, corresponding to ~ 1050 rpm of the 3-phase synchronons motor driving the chopper. The resulting (velocity-independent) resolution was $\Delta v/v \simeq 5\%$; the (vertical) flight path was (10.96 ± 0.01) m. A 256 channel multiscaler was used with scaler frequency 920.0 cps giving a channel width $\simeq 0.39$ Å. The overall open beam detector count rate integrated over the spectral range 11–47 Å was $\simeq 6000$ cpm. The background-to-open-beam ratio was less than 0.01% for the whole range except near 11 Å where it amounted to $\sim 0.02\%$. This allowed the evaluation of data even for rather thick samples with transmissions as low as $\sim 1\%$.

The cobalt sample was a 0.02″ sheet, spec. pure, with $n = (4.645 \pm 0.003) \cdot 10^{-3}$ atoms/b. For gold we used the same 0.88 mm sample (Section II.3) that had been also used in the 4–7.6 Å range. Data for wavelengths above ~ 20 Å were obtained with a 0.25 mm thick sample (purity 99.999%), with $n = (1.5137 \pm 0.0015) \cdot 10^{-3}$ atoms/b.

The analysis of the TOF spectra was done by evaluating again for each channel the total cross section and wavelength. Cross sections were calculated in the usual way considering background and dead time corrections; reflexion losses at the entrance and exit surfaces of the samples (Steyerl and Vonach [28]) are still negligible at wavelengths below 50 Å. The effects of thermal inelastic and incoherent elastic "in-scattering" from sample to detector were estimated for the given geometry (sample-detector distance 25 mm, detector window 13 mm ∅), but were found to be also negligible for gold and cobalt even at transmissions near 1%.

The wavelength corresponding to each channel was calculated from the flight path and the time-of-flight with consideration of the following points: (1) Because of the *vertical* arrangement of the spectrometer neutrons are decelerated along the flight path, because of gravity. This introduces a slight deviation from the linear relation between time-of-flight and wavelength at the detector, which can be calculated in a straighforward manner, and was at most 0.8% (47 Å). (2) The wavelengths were corrected for the effect of intensity asymmetry within the resolution width, which slightly shifts the effective wavelength of a time channel from the channel center towards the maximum of intensity. The correction was $\lesssim 0.1\%$ throughout the range 11–47 Å. (3) At long wavelengths the neutron optical effect of refraction must be accounted for, i.e. the difference between the vacuo wavelength measured by time-of-flight, and the wavelength within the sample medium which deter-

mines the absorption [28]. This was considered in the normalization of the absorption per Å, however, the correction was at most 0.2% (gold, 47 Å). The normalized absorption was again calculated as

$$(\sigma_{\text{tot}}-\sigma_{\text{inc}}-\sigma_{\text{ie}})^i/\lambda^i$$

using the scattering data given in Section II.5. Weighted means over each ~ 3.5 Å range (nine channels) are given in Table 2. Wavelength errors are estimated considering the uncertainty of the flight path which produces the same relative error of 0.1% for all wavelengths, and the uncertainty in the zero of the time-of-flight scale (<100 μs) which produces an additional (absolute) error of 0.04 Å for all wavelengths.

The combined results of our measurement in the range 11–47 Å are

$$\text{Au } \sigma_a/\lambda=(54.46\pm 0.15)\text{ b/Å},$$

$$\text{Co } \sigma_a/\lambda=(20.64\pm 0.06)\text{ b/Å}.$$

The quoted errors are calculated from the quadratic sum of the statistical uncertainty (Au 0.17%, Co 0.2%) and the estimated errors of sample thickness (Au 0.1%, Co 0.07%) and wavelength measurement (~ 0.2%).

IV. Summary

Gold: Total cross sections have been measured in the wavelength range 4–7.6 Å using a new time-of-flight spectrometer which provided high wavelength resolution and accuracy, excellent background conditions and sufficient intensity for precision measurements. Thus, we believe our final results for the absorption (Section II.5.1) to be accurate within ~ 0.1%. Our data do not support a significant wavelength trend found in a previous measurement [6].

A supplementary transmission measurement was done in the range 11–47 Å. The result was slightly higher but consistent within statistics and the larger experimental uncertainties at these wavelengths. Thus, our data indicate no significant deviation from the expected variation of the absorption at low energies. Using the result of Section II.5.1

$$(\sigma_a/\lambda)_0=(54.35\pm 0.06)\text{ b}$$

the extrapolation to 2200 m/s (1.798_2 Å) gives 97.73 b for the λ-proportional absorption. The non-λ-proportional absorption at thermal energy caused by the 4.906 eV level is (0.95 ± 0.04) b, on the basis of the single level Breit-Wigner formula and the parameters of Wood *et al.* [22]. Thus we obtain for the thermal capture cross section

$$\sigma_a(2200\text{ m/s})=(98.68\pm 0.12)\text{ b},$$

to be compared with the previous results given in Table 3.

Cobalt: Our results for the two wavelength ranges (Sections II.5.2, III) are of the same accuracy and can be considered as independent, since the principal systematic uncertainties were different in both ranges. The mean is

$$\sigma_a/\lambda = (20.65_7 \pm 0.04)\ \text{b/Å},$$

$$\sigma_a(2200\ \text{m/s}) = (37.15 \pm 0.08)\ \text{b}.$$

This should be compared with the value (37.55 ± 0.13) b recommended by Story [29] on the basis of nineteen measurements prior to 1968, and with the most recent results (37.35 ± 0.30) b (Vaninbroux [30]), (37.14 ± 0.27) b (Merrit and Green [31]) and (37.245 ± 0.11) b (Silk and Wade [10]).

The authors wish to acknowledge gratefully the current support and interest by Professor H. Vonach, who stimulated this work. Thanks are also due to Dr. A. Steyerl for valuable discussions and advice in the measurements at his ultra-cold-neutron spectrometer. Mr. W. Waschkowski was so kind to perform the cobalt measurement at 1.25 eV. Mr. K. Färber kindly assisted in the operation of the three-chopper system.

References

1. Stehn, J. R., Goldberg, M. D., Magurno, B. A., Wiener-Chasman, R.: BNL 325, 2d ed., suppl. N2 (1966)
2. Gibbons, J. H.: Conf. Neutron Cross Sections and Technology, Washington, Vol. I, 111 (1968)
3. Vlasov, M., Dunford, C., Schmidt, J., Lemmel, H.: INDC (NDS)-47/L (1972)
4. Gould, F. T., Taylor, T. I., Havens, W. W., Rustad, B. M., Melkonian, E.: Nucl. Sci. Eng. **8**, 453 (1960)
5. Teutsch, H., Matescu, N., Timis, P.: Nukleonik **4**, 165 (1962)
6. Als-Nielsen, J., Dietrich, O.: Phys. Rev. **133**, B 925 (1964)
7. Prosdocimi, A., Deruytter, A.: J. Nucl. Energy **17**, 83 (1963)
8. WRENDA 73, World Request List for Neutron Data Measurements for Nuclear Reactors, INDC (SEC)-32 U (1973), request No. 782
9. Carter, R. S., Palevsky, H., Myers, V. M., Hughes, D. J.: Phys. Rev. **92**, 716 (1953)
10. Silk, M. G., Wade, B. O.: J. Nucl. Energy **24**, 43 (1969)
11. Wu, C. S., Rainwater, L. J., Havens, W. W.: Phys. Rev. **71**, 174 (1947)
12. Bernstein, S., Borst, L. B., Stanford, C. P., Stephenson, T. E., Diel, J. B.: Phys. Rev. **87**, 487 (1952)
13. Steichele, E., Arnold, P.: Phys. Lett. **44A**, 165 (1973)
14. Maier-Leibnitz, H.: Proc. Int. Symp. on Neutron Capture Gamma Ray Spectroscopy, p. 93. Studsvik (1969)
15. Simpson, O. D., Marshall, N. H., Young, R. C.: Nucl. Instr. Methods **16**, 97 (1962)
16. Wyckof, F.: Crystal Structures, 2d ed., Vol. I (1965)
17. Egelstaff, P. A., Pease, R. S.: J. Sci. Instr. **31**, 207 (1954)
18. Weiss, J. R.: Phys. Rev. **86**, 271 (1952)
19. Brockhouse, B.: See footnotes p. 720 of [9] and p. 644 of [22]
20. Kothari, L. S., Singwi, K. S.: Proc. Roy. Soc. (London), Ser. A **231**, 293 (1955)
21. Binder, K.: phys. stat. sol. **41**, 767 (1970); and Report PTHM-FRM-110

22. Wood, R. E., Landon, H. H., Sailor, V. L.: Phys. Rev. **98**, 639 (1955)
23. Moon, R. M.: Phys. Rev. **136**, A 195 (1964)
24. Roth, W. L.: Phys. Rev. **110**, 1333 (1958)
25. Fehsenfeld, P.: Thesis, Technische Universität München (1971)
26. Waschkowski, W.: Unpublished
27. Steyerl, A.: Nucl. Instr. Methods **101**, 295 (1972)
28. Steyerl, A., Vonach, H.: Z. Physik **250**, 166 (1972)
29. Story, J. S.: AEEW-R 597 (1968)
30. Vaninbroux, R.: Nucl. Sci. Eng. **24**, 87 (1966). Author reported $\sigma_{act}=37.4$ b; the value given in the text is the *absorption* as corrected by Story [29]
31. Merrit, J. S., Green, R. E.: Can. J. Phys. **46**, 2325 (1968)

Dr. W. Dilg
Dipl.-Phys. W. Mannhart
Dr. E. Steichele
Dipl.-Phys. P. Arnold
Physik-Department (E 14)
der Technischen Universität München
D-8046 Garching bei München
Reaktorstation
Federal Republic of Germany